Hindawi
International Journal of Antennas and Propagation
Volume 2022, Article ID 9078929, 13 pages
https://doi.org/10.1155/2022/9078929

Research Article

Four Element MIMO Antenna Systems with Decoupling Lines for High-Speed 5G Wireless Data Communication

Imaculate Rosaline,[1] Arvind Kumar,[2] Prashant Upadhyay,[3] and Abu Hena Murshed[4]

[1]*Department of ECE, Ramaiah Institute of Technology, Bangalore, India*
[2]*Department of Electronics and Communication Engineering, Visvesvaraya National Institute of Technology, Nagpur 10, India*
[3]*Madanapalle Institute of Technology and Science, Madanapalle, Andhra Pradesh, India*
[4]*Chittagong University of Engineering & Technology, Chittagong, Bangladesh*

Correspondence should be addressed to Abu Hena Murshed; u1508017@student.cuet.ac.bd

Received 29 March 2022; Revised 24 May 2022; Accepted 31 May 2022; Published 25 June 2022

Academic Editor: Eng Hock Lim

A low-profile planar multiple-input multiple-output (MIMO) antenna consisting of four elements with isolation improvement is proposed for 5G mm Wave (24–40) GHz applications. Each radiating element of the MIMO antenna comprises of a microstrip-fed tilted spade-shaped radiator with four asymmetrical slots and a partial ground plane. The antenna is optimized to resonate at 35 GHz covering a wide impedance bandwidth from 23.9 to 40.1 GHz. Two cross lines are then loaded between the antenna elements to improve the isolation > -30 *dB*. The MIMO structure with the decoupling lines is fabricated and tested. The measured results are in good correlation with the simulated results. Other MIMO performance metrics such as the envelope correlation coefficient (ECC), channel capacity loss (CCL), diversity gain (DG), and total active reflection coefficient (TARC) are examined, and the results are found to be satisfactory for the device to be used for mm-wave 5G MIMO applications. Also, the antenna's performance metrics such as radiation efficiency, gain, and radiation patterns over the operating band are presented.

1. Introduction

The evolution of the cellular technology, from analog to 5G, has been a long road, requiring an out-of-box solution for wireless ultrahigh-speed data transmission. The 5G story will be one of momentum, evolution, and transformation, leading to an even more connected world, extending beyond consumers to industrial applications and defence-oriented niche applications to an enabling technology used in mobile handheld devices. 5G is being deployed worldwide using sub-6 GHz and mm Wave frequency ranges. The fifth-generation will be a mobile network and, unlike its predecessors, including 4G, 3G, and 2G; it aims to be an "everything network," that is, available "everywhere" for "everyone" able to facilitate high-speed data rates with minimal power consumption [1–5]. The International Telecommunication Union (ITU) has announced quite a few 5G bands among several countries for cellular communication which varies from 24.25 GHz to 43.5 GHz as discussed in [6]. Thus, RF components design pertaining to millimetre wave (mm Wave) and submillimetre wave bands which have gained lot of attention among researchers globally. However, certain limitations such as signal fading and path loss attenuations occur with single antenna elements at such high frequencies [7, 8]. In such situations, multiple-input multiple-output (MIMO) antenna systems are found to be a promising technology. It increases channel capacity thus enabling high data rates [9–11, 40–49].

Mobile service base stations find MIMO antenna systems to be incorporated with ease. Several designs of MIMO antenna systems for 5G applications have been proposed in the literature. [12–18]. Few notable works based on different structures are PIFA pair-based MIMO configuration [12], EBG-based MIMO antennas [13, 14], DRA-based antennas [15, 16], MIMO-based slot antenna arrays for 5G exhibiting a wide mm Wave band resonance from 22.5 to beyond

50 GHz [17], CSRR-loaded *T*-shaped MIMO antenna [18], and a MTM- and SIW-inspired MIMO antenna with AMC [19]. However, many of these antennas suffer limited bandwidth and complex geometry. The design of wideband and multiband 5G mm Wave MIMO antennas has attracted many researchers in recent times. A defected ground structure (DGS) based 4 ports MIMO antenna [20] shows resonance from 25.1 to 37.5 GHz. A wideband 8-port MIMO antenna covering a wide band from 27.4 to 28.23 GHz is discussed in [21]. A SIW cavity-backed antenna [22] is proposed to cover mm Wave bands ranging from 27.55 to 62.32 GHz. Few other antennas proposed in [23, 24] discussed MIMO antenna systems resonating at both sub-6 GHz frequency range like 2–5 GHz and also in the higher frequency mm Wave range like 23–29 GHz [25].

Nevertheless, the design of MIMO antenna systems for user interface components faces several encounters, such as the requirement of high bandwidth, high gain, and compactness of the structure. Apart from these, the main challenge lies in the design of closely packed antennas with low mutual coupling and high isolation, more the number of independent antennas, the higher the data rate transmission. The size of the mobile builds a limitation on the distance between the antenna elements. Thus, the arrangement of MIMO antennas with high isolation within the available space of a compact mobile phone or laptop is necessary [26]. Many isolation enhancement techniques have been discussed in the literature. Orthogonal polarization [27], metamaterial inspired split-ring resonators [28, 29], decoupling elements [30], defected ground structures and layered substrate configuration [31, 32], neutralization lines [33, 34], and self-isolated antenna [35–38] are few among them. To this end, the design of a four-element MIMO antenna with decoupling lines is proposed in this paper. The antenna is optimized to resonate at 35 GHz with a wide impedance bandwidth 23.9 to 40.1 GHz (16.2 GHz). The isolation between the antennas is improved by using a simple decoupling structure between them. The design of the single antenna element and its parametric analysis of the return loss characteristics are discussed in Sections 2 and 3, respectively. The orthogonal arrangement of the four elements MIMO system and the design of the decoupling structure are discussed in Sections 4 and 5, respectively. The radiation pattern and the MIMO parameter discussion are given under Sections 6 and 7, respectively.

2. Single-Element Antenna Design and Its Working Principle

The proposed single-element radiator consists of a tilted spade-shaped patch printed on a $5.5 \times 4.4\,\text{mm}^2$ Rogers RO4003 substrate, whose dielectric constant ε_r is 3.55, loss tangent is 0.0027, and height is 0.787 mm. Figure 1 shows the geometrical layout of the proposed antenna, and Figure 2 shows the evolution process. In configuration A, a spade-shaped patch element whose tip is slightly tilted is chosen as the main radiator. This element is fed by 1.1 mm × 1.375 mm, 50 Ω microstrip feed line, and backed by a partial ground plane. Upon excitation, it yields a resonance around 42 GHz, with an impedance bandwidth from 36.28 GHz to 43.3 GHz. This response is mainly contributed by the feed length and the circumferential length of the spade radiator. As observed in Figure 3(a), the simulated surface current distribution shows a dense current flow along the transition section of feed line to the main radiator. An out-of-phase current flow is observed at a distance of around 1 mm from the feed location which corresponds to $\lambda_g/4$ at the resonant frequency. Also, in Figure 3(b), the simulated electric field distribution is shown, in which a "*V*"-shaped sparse vector field is located. This led to the evolution of configuration B, where two "*V*" shaped slots with width "*g*" inclined at an angle of 5° to the right and 32° to the left from the centre of the patch are introduced. The slots tend to improve the impedance matching at the operating frequency without much altering the resonance. The width of the slots is tuned to achieve the optimum impedance matching condition. Later, a rectangular patch of dimensions $1.54 \times 1.925\,\text{mm}^2$ is added at a distance of Lg from the feed point, which contributes for more concentrated field distribution along the open ends of the slot in the patch, rather than at the centre. Open end of the slot reduces its *Q* factor and leads to a wider bandwidth [37–39]. This in turn leads to the shift in the resonant frequency to around 34 GHz from 42 GHz. Finally, in the proposed design, the feed width is altered by introducing a step feed at a distance of fL2 from the feed point, to improve the impedance matching. Thus, the proposed single element exhibits a resonance at 35 GHz (23.9–37.3) GHz. The simulated return loss characteristics of all the configurations involved in the evolution of the final proposed element are shown in Figure 4. The parameters of the antenna are fine-tuned to obtain the expected results and are listed in Table 1.

3. Parametric Analysis on the Single Element

The simulations are performed in the commercially available EM tool Ansys HFSS 2018.1. There are several parameters that influence the operating frequency. Figure 5 shows the variation of parameters "*g*" (slot width), "fw2" (step feed width), "L" (distance from feed point to the slot) vs. frequency. Parameter *g*' is varied from 0.2 mm to 0.5 mm in steps of 0.1 mm, fw2 is varied from 1.70 mm to 1.79 mm in steps of 0.3 mm, and *L* is varied from 3.19 mm to 3.25 mm in steps of 0.2 mm. It is inferred that increasing values of *g* and fw2 shift the resonant frequency from lower to higher values, whereas increasing *L* value retains the resonant frequency at 35 GHz but offers reduced impedance matching.

4. Four Port Orthogonal MIMO Configuration

A 4 port orthogonal MIMO arrangement is shown in Figure 6, and it occupies an area of $13.75 \times 13.75 \times 0.787 mm^3$. The antennas are placed at a distance 4 mm ($\lambda/2$) in *x* and *y* directions. The distance between the antenna elements plays a significant role in determining the mutual coupling. For any shorter distances than 4 mm, electromagnetic energy from the excited patch gets coupled to the nearby radiating element so mode separation happens in the lower frequency region as shown in Figure 7. The figure shows the simulated

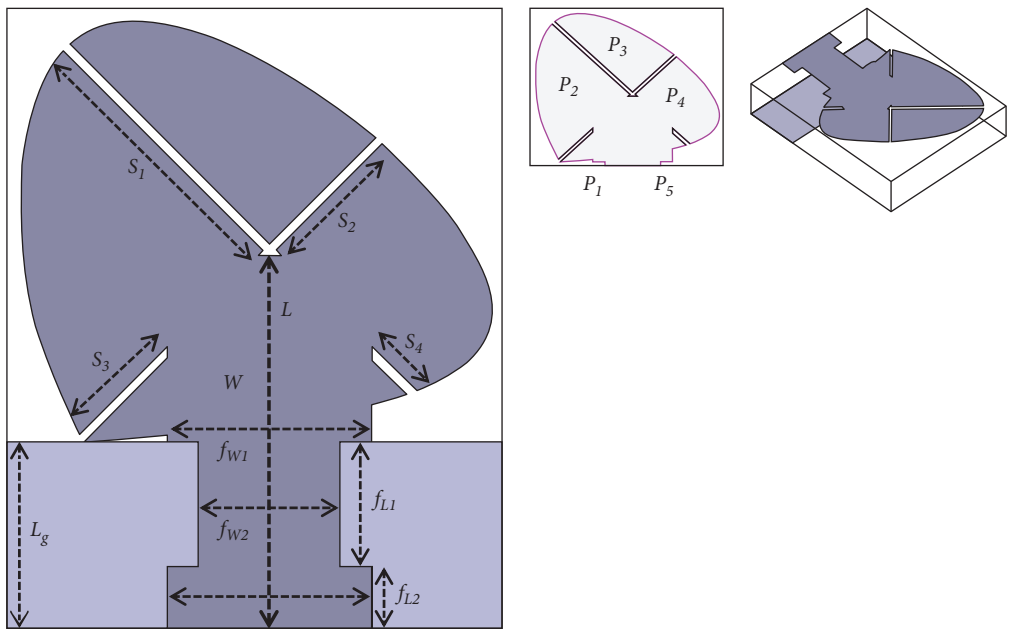

Figure 1: (a) Geometrical layout of the proposed single element. (b) Outline of the titled patch. (c) Perspective view of the proposed single element.

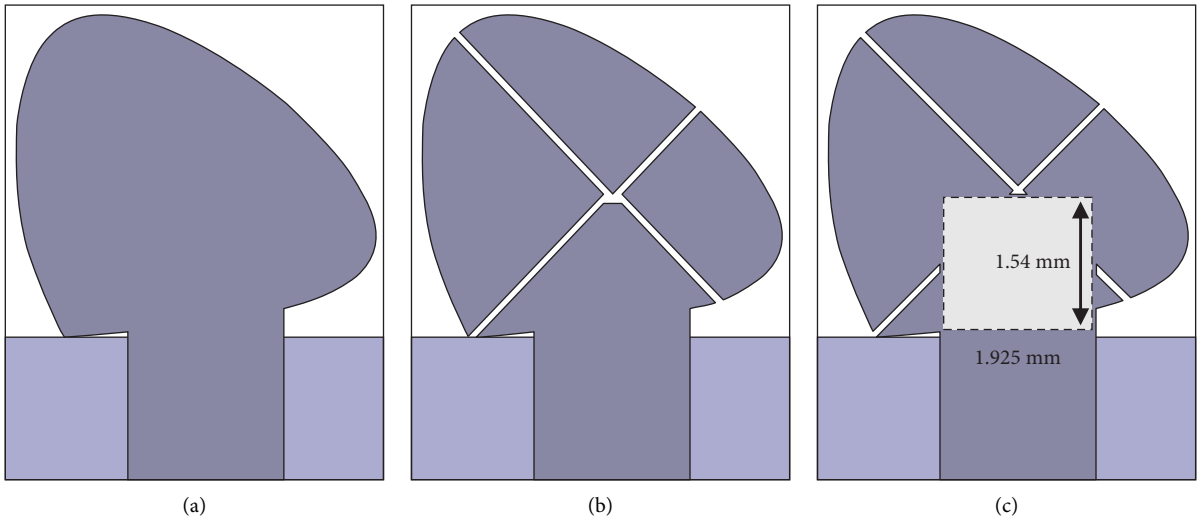

Figure 2: Continued.

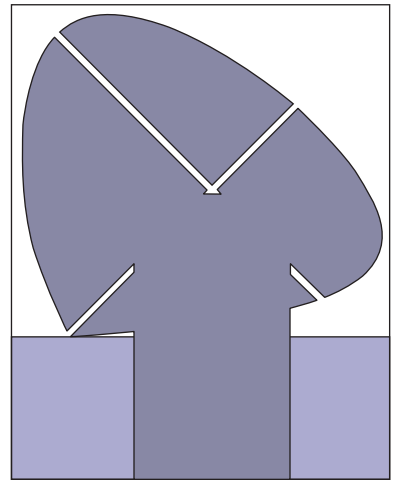

(d)

Figure 2: Evolution of the proposed antenna. (a) Config A, (b) config B, (c) config C, (d) config D.

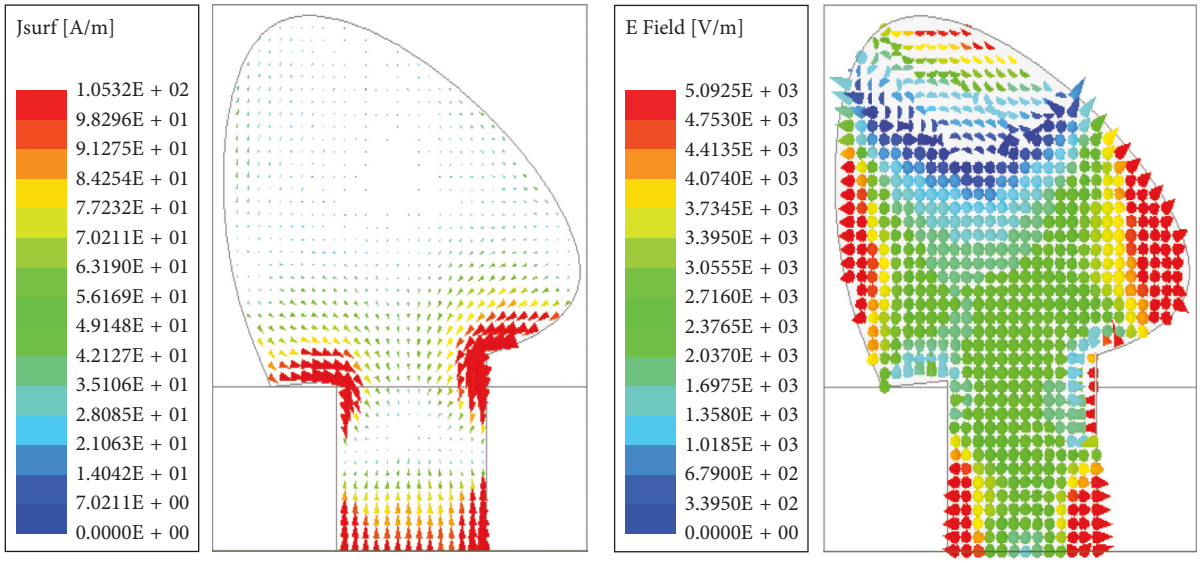

(a) (b)

Figure 3: Simulated (a) electric field distribution and (b) surface current distribution of the proposed single element at 42 GHz.

return loss characteristics of the proposed MIMO configuration for various distances from 3.5 mm to 5.0 mm in steps of 0.5 mm. It is observed that for a distance of 4.0 mm, the resonance of the antenna is well preserved as that of the single element, and for any of the incrementing distances, the impedance match is lost. Thus, an optimum distance of 4.0 mm along x and y directions is chosen. Figure 8 shows the simulated S parameters of the proposed MIMO configuration with Port 1 ON and all other ports OFF. The S_{11} (dB) is observed to show resonance from 24 GHz to 39.6 GHz. A maximum isolation of around −25 dB is achieved at 35 GHz from port 2, and a minimum isolation of around −28 dB is achieved from port 3 at the resonating frequency. Figure 9 shows the simulated surface current distribution on the proposed MIMO configuration with each ports ON and OFF individually. When each port is excited, we could visualize the current distribution only along that particular patch and moderate coupling to the adjacent antenna elements. Figure 10 shows the simulated return loss characteristics along all the 4 ports. The resonance at 35 GHz remains unaltered.

5. MIMO Structure with Decoupling Lines

To further improve the isolation between the antennas, a simple decoupling element comprising of two cross lines is used. The cross lines run between the antenna elements adjacent to each other as shown in Figure 11. The width of the decoupling line is optimized to be 2 mm. An increase or decrease in this parameter greatly affects the resonant

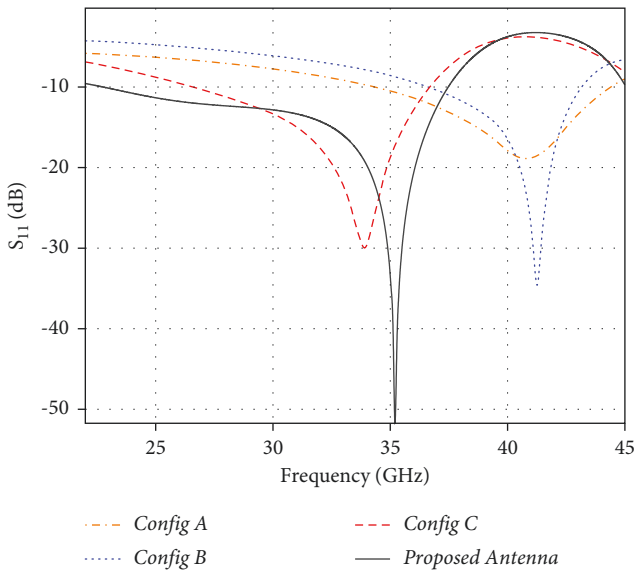

Figure 4: Simulated return loss parameters of the several configurations given in Figure 2.

Table 1: Dimensions of the proposed single element.

P1	*P2*	*P3*	*P4*	*P5*	*S1*	*S2*	*S3*
1.03	3.57	3.02	2.83	0.91	2.51	1.36	1.16
S4	*L*	*W*	*fL1*	*fL2*	*fW1*	*fW2*	*Lg*
0.62	3.19	1.76	1.1	0.55	1.21	1.76	1.65

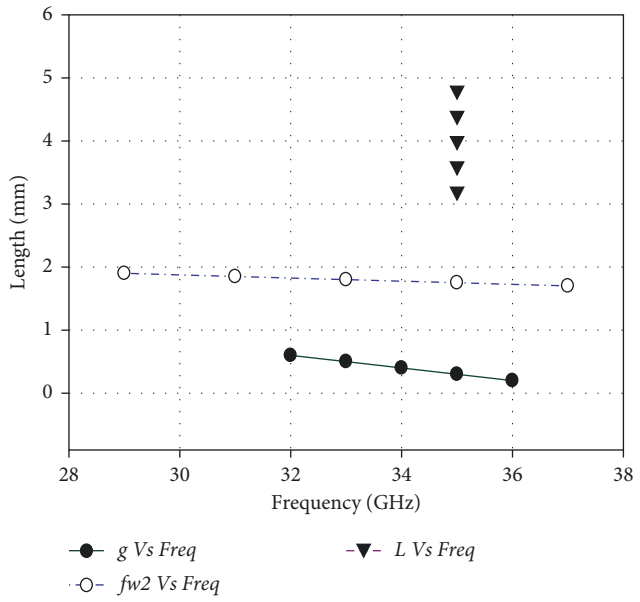

Figure 5: Variation of parameters "g", fw2′, and L vs. frequency.

behaviour which is shown in Figure 12. The width of the line is varied from 1 mm to 4 mm in steps of 1 mm, and the optimum is chosen as 2 mm. The decoupling line has improved the isolation by reducing the surface wave propagation inside the substrate and space wave propagation

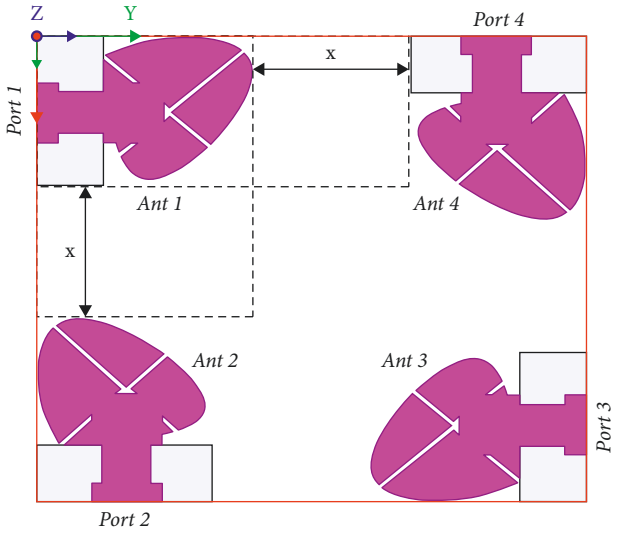

Figure 6: 4 port orthogonal MIMO configuration.

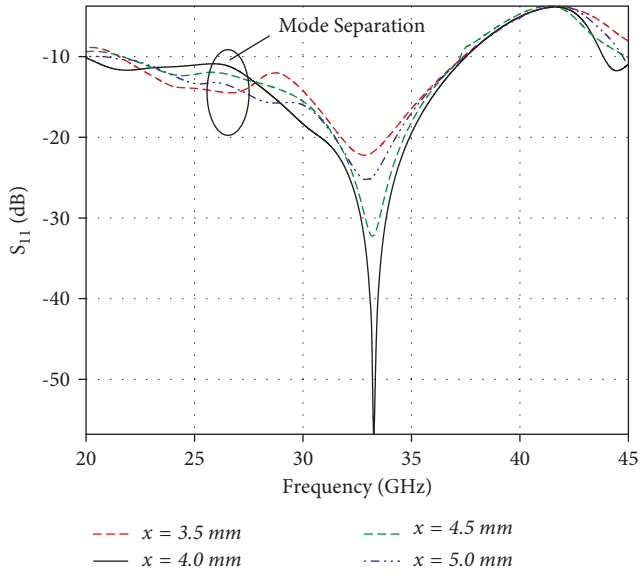

Figure 7: Simulated return loss characteristics of the proposed MIMO configuration for various values of distance "x".

related to the reactive coupling of nearby radiating elements. These lines excite orthogonal modes in the adjacent ports leading to low mutual coupling. This can be well understood by the surface current distribution of the MIMO configuration along with the decoupling structure, which is shown in Figure 13. It shows the surface current distribution under 4 conditions where each port is made ON, when the other remaining ports are made OFF. The current is dense only along the radiating element where excitation is applied, and all other radiating elements have very sparse current distribution, which validates the mutual coupling reduction. The transmission parameters between ports 1 and 2, 1 and 3, 1 and 4 with and without the decoupling line are shown in Figure 14 for comparison. Mutual coupling between the antennas has reduced from around −20 dB to −30 dB over the entire operating band. A prototype of the final optimized

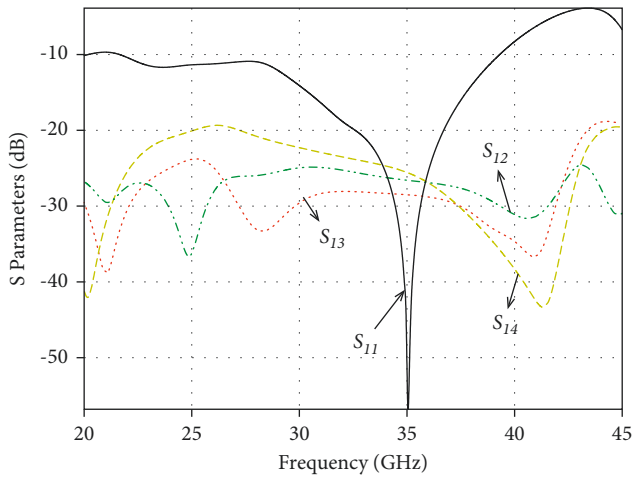

Figure 8: Simulated return loss and transmission parameters of the proposed MIMO configuration.

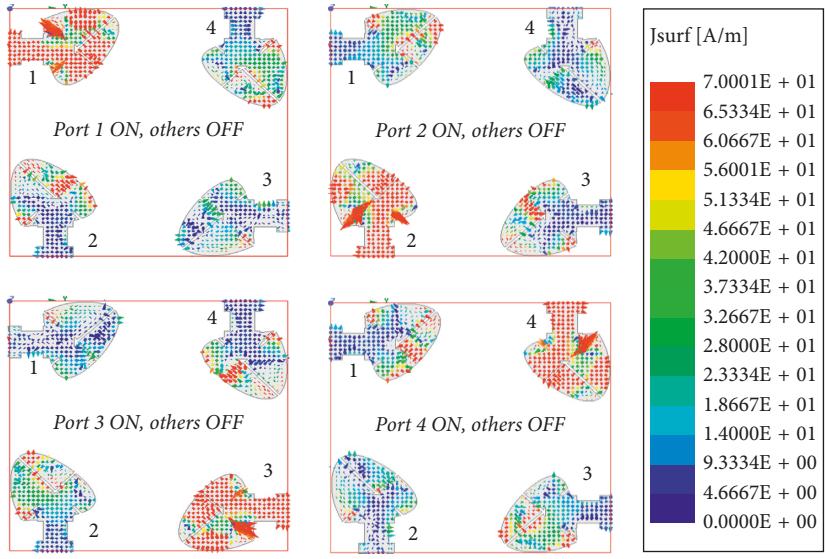

Figure 9: Simulated surface current distribution on the MIMO configuration. (a) PORT 1 ON, others OFF. (b) PORT 2 ON, others OFF. (c) PORT 3 ON, others OFF. (d) PORT 4 ON, others OFF.

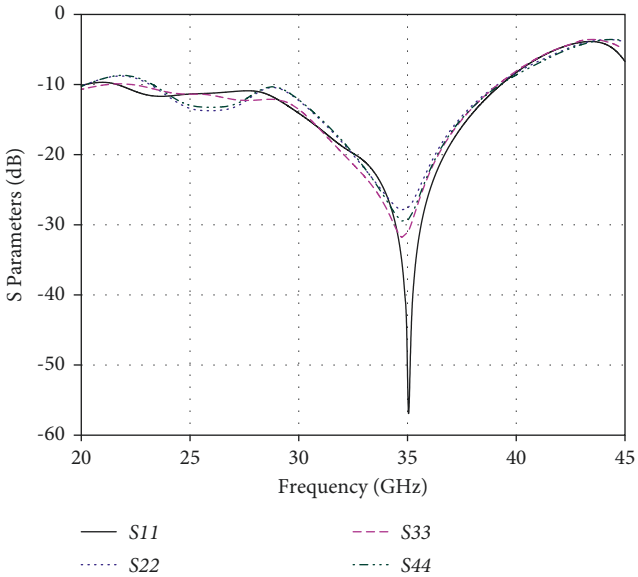

Figure 10: Simulated return loss characteristics of the proposed MIMO configuration at each port.

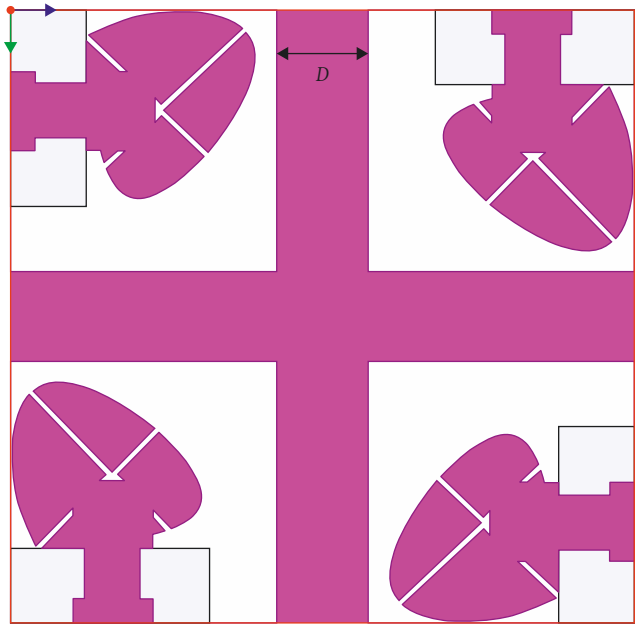

Figure 11: Proposed MIMO configuration with the decoupling lines.

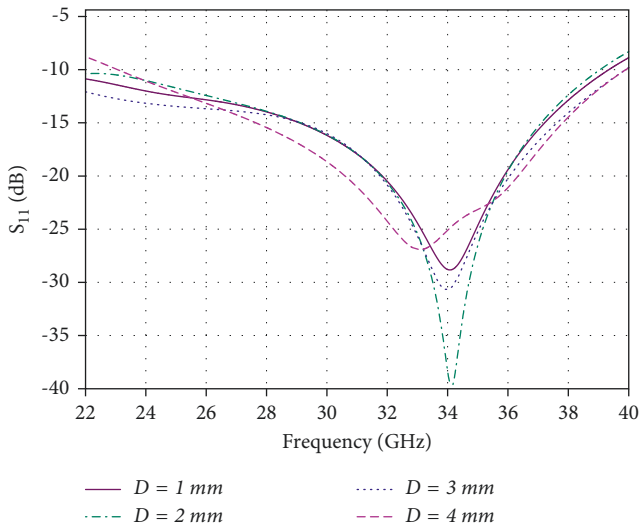

Figure 12: Simulated return loss characteristics of the proposed MIMO system for various values of 'D'.

MIMO system with the decoupling lines are fabricated and the photograph of the same is shown in Figure 15(a). The measured S parameters are shown in Figure 15(b), from where it is inferred that both the results fairly match with each other, making the proposed MIMO system suitable for 5G mm-wave applications.

6. Radiation Pattern, Gain, and Efficiency

The radiation pattern of the proposed MIMO configuration with the decoupling line is measured using the commercial far-field measurement system in an anechoic chamber. Field pattern is measured both along XZ and YZ planes with theta ranging from 0° to 360°. Figure 16 shows the measured co-pol and cross-pol radiation pattern of antenna 1 and 3 at 35 GHz. Since the antenna arrangements are symmetric along the centre, a similar radiation pattern is expected from the other two antennas (2 and 4) and so they are not shown. It is seen from the figure that both antennas exhibit almost omnidirectional radiation at the operating frequency, which is very important to make the proposed design a suitable one for wireless applications. Figure 17 shows the measured gain and radiation efficiencies of antennas 1–4. It is observed that the measured gain values are between 3 and 5 dB, and the radiation efficiencies are between 65 and 85% within the entire bandwidth which is satisfactory for 5G MIMO applications.

$$DG = 10\sqrt{1 - |ECC|^2}. \quad (3)$$

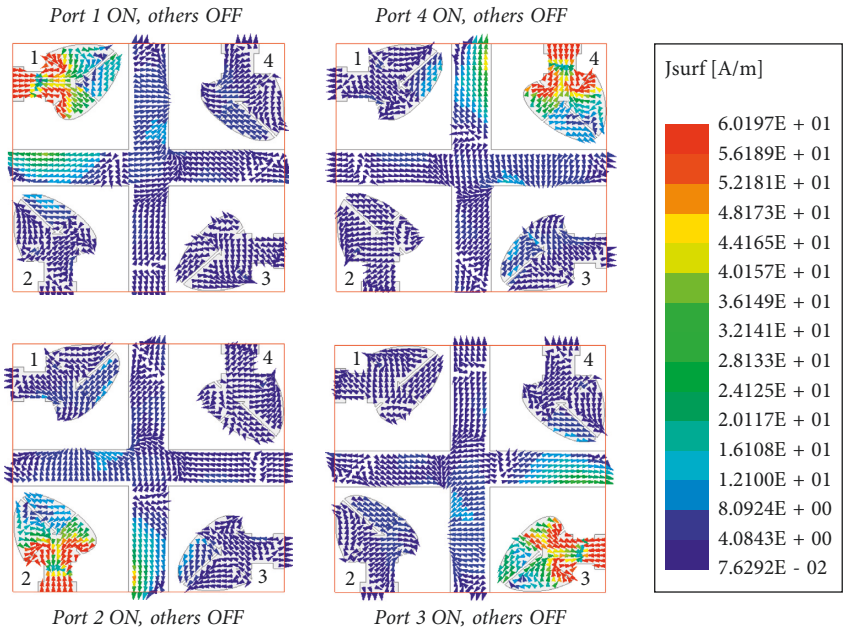

Figure 13: Simulated surface current distribution on the MIMO configuration with decoupling lines.

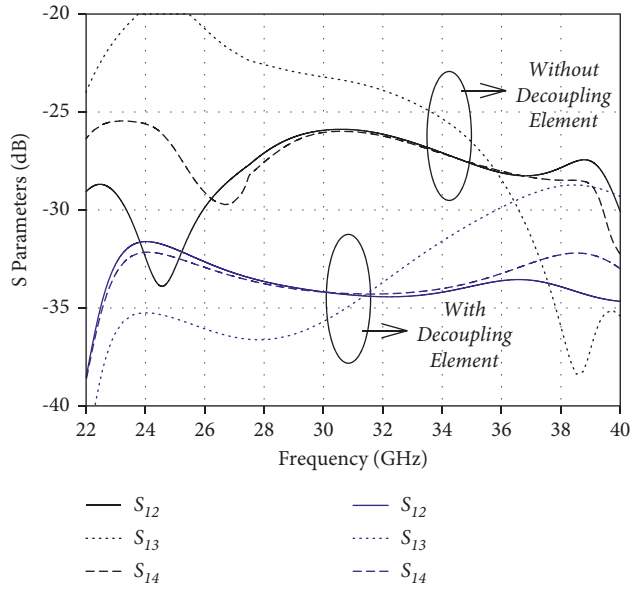

Figure 14: Simulated S parameters of the proposed MIMO configuration with and without decoupling lines.

7. MIMO Parameters

Few MIMO performance metrics such as ECC, DG, TARC, and CCL ensure the multichannel performance of the proposed antenna. Thus, these parameters are analysed individually for the proposed MIMO antenna and given below.

7.1. Envelope Correlation Coefficient (ECC). The ECC defines how independent each antenna's radiation patterns are. It is calculated using the following formula:

$$\rho_{ij} = \frac{\left|S_{ii}^{*}S_{ij} + S_{ji}^{*}S_{jj}\right|}{\left(1 - \left|S_{ii}\right|^{2} - S_{ij}^{2}\right)\left(1 - \left|S_{ji}\right|^{2} - S_{jj}^{2}\right)}. \quad (1)$$

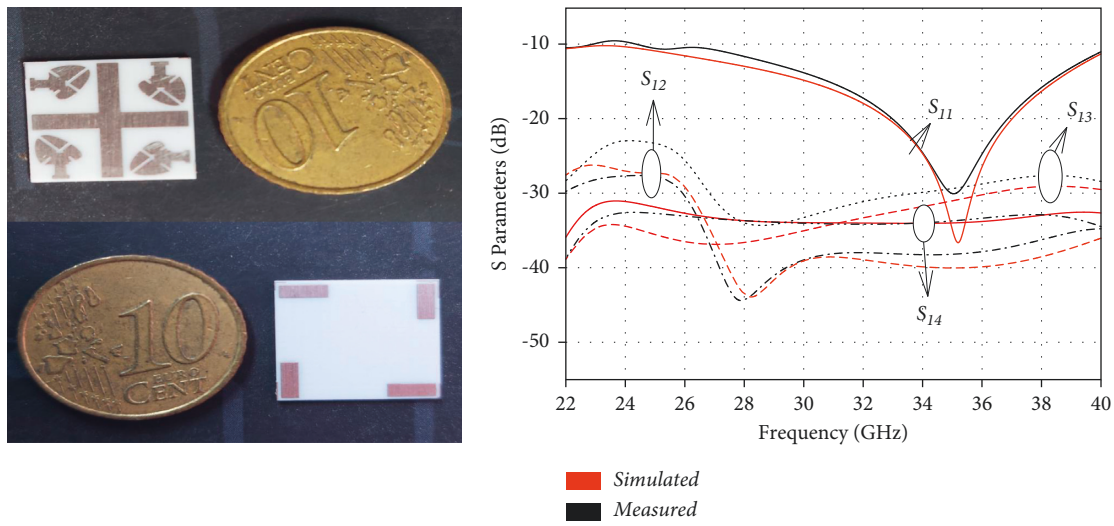

FIGURE 15: (a) Fabricated prototype of the proposed MIMO antenna with decoupling lines. (b) Simulated and measured S parameters of the MIMO configuration with decoupling lines.

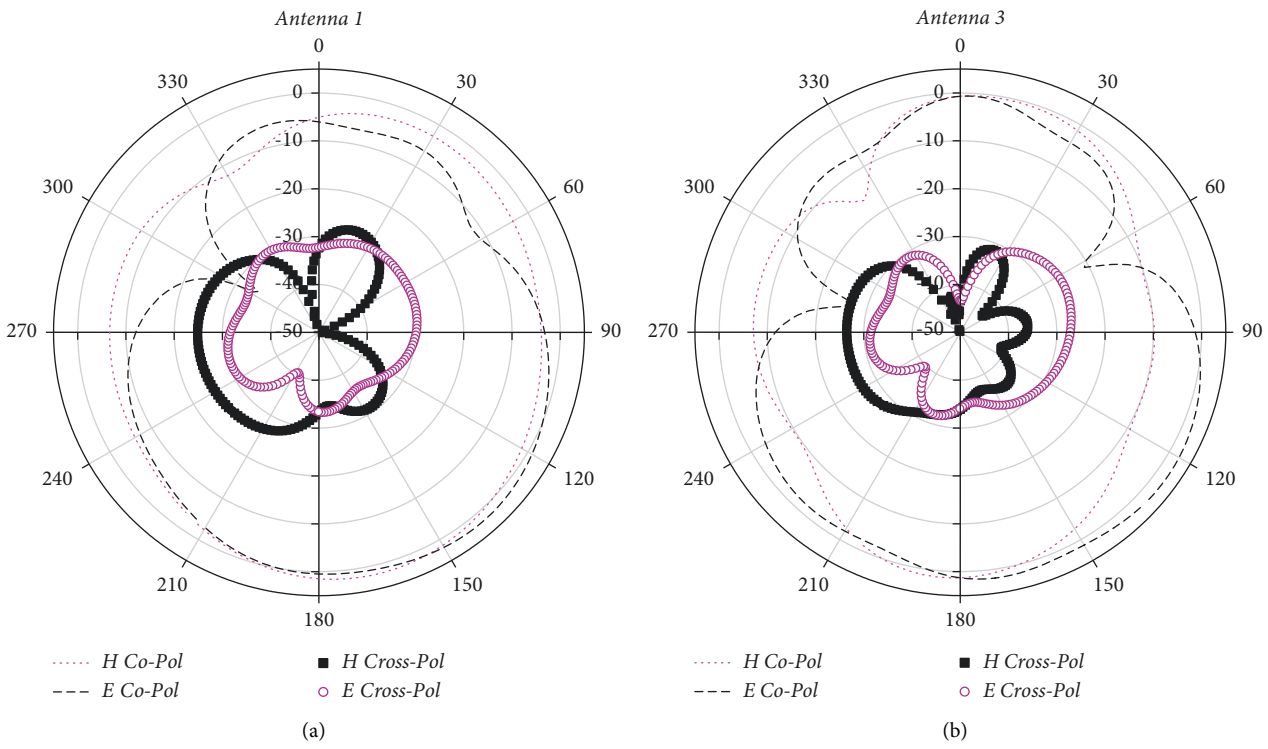

FIGURE 16: Measured radiation patterns of antennas 1 and 3 at 35 GHz.

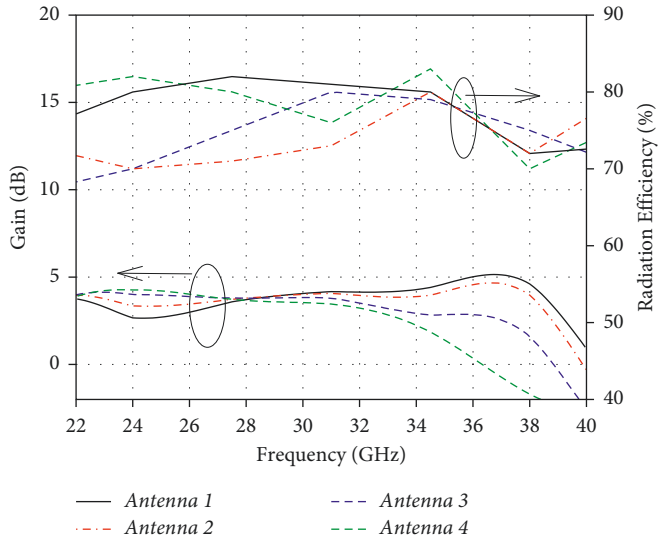

Figure 17: Measured gain and radiation efficiencies of antennas 1–4.

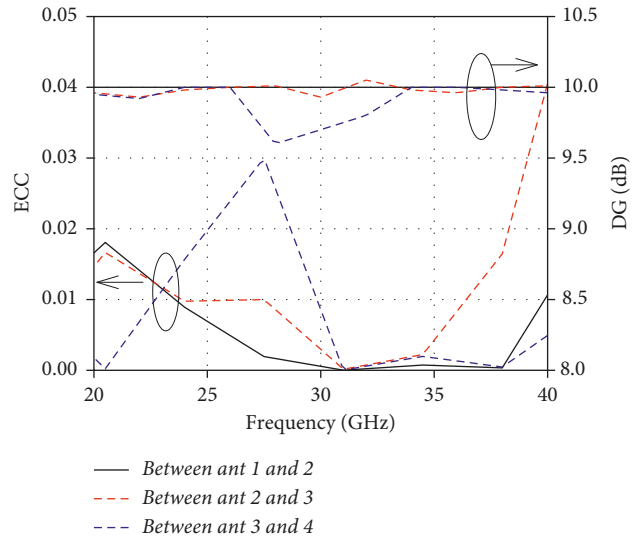

Figure 18: Calculated ECC and DG (dB) between antennas 1 and 2, 2 and 3, 3 and 4.

Figure 18 shows the calculated ECC between antennas 1 and 2, 2 and 3, 3 and 4. The overall correlation values lie below the practical standard of 0.5.

The ECC of a MIMO antenna using the radiation pattern is given as [49]

$$\rho_{12} = \left| \frac{\int_0^{2\pi}\int_0^{\pi}\left(XPR.E_{\theta i}.E_{\theta j}^{*}.P_{\theta} + XPR.E_{\varphi i}.E_{\varphi j}^{*}.P_{\varphi}\right)\sin\,\theta\,d\theta\,d\varphi}{\sqrt{\prod_{k=i,j}\int_0^{2\pi}\int_0^{\pi}\left(XPR.E_{\theta k}.E_{\theta k}^{*}.P_{\theta} + XPR.E_{\varphi k}.E_{\varphi k}^{*}.P_{\varphi}\right)\sin\,\theta\,d\theta\,d\varphi}} \right|^{2}. \quad (2)$$

Here, XPR is the cross-polarization ratio of vertical and horizontal polarized components. P_θ and P_φ represent the angular power spectrum of the propagation environment, $E_{\theta i}, E_{\theta j}, E_{\varphi i}, E_{\varphi j}$ represent the far-field components in the θ plane and φ plane, respectively. The ECC is calculated between antennas 1 and 2 using the above expression and is shown in Figure 18. The obtained ECC lies below the expected value of 0.5, because the antennas have high isolation between them, as confirmed by the S parameter results.

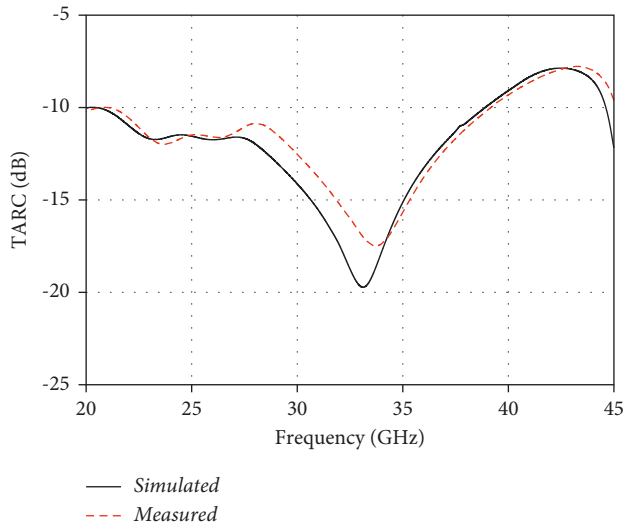

Figure 19: Simulated and measured TARC vs. frequency.

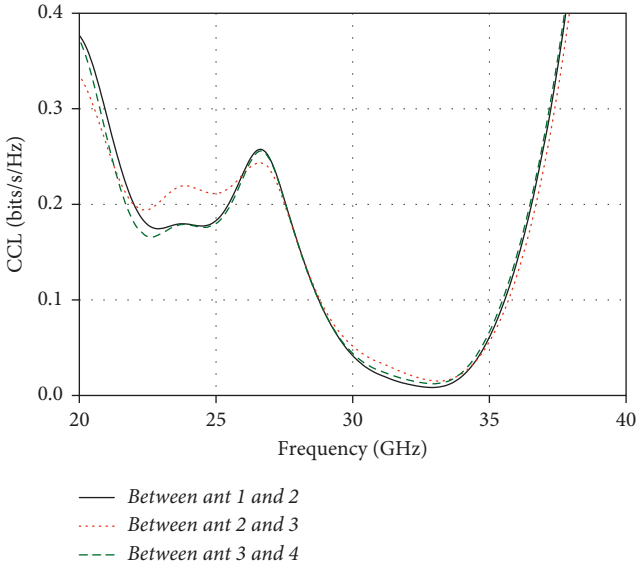

Figure 20: Calculated CCL (bits/s/Hz) between antennas 1 and 2, 2 and 3, 3 and 4.

7.2. Diversity Gain (DG). The DG signifies the signal-to-noise ratio (SNR) improvement in the MIMO system as compared with the single antenna. The ideal value of DG (dB) is 10. It is calculated using the formula.

Figure 18 shows the DG (dB) calculated between antenna elements 1 and 2, 2 and 3, 3 and 4. It is seen that the DG value varies between 9.6 and 10 which is very close to the ideal value as anticipated.

7.3. Total Active Reflection Coefficient (TARC). The TARC defines the return loss of the entire MIMO array and in turn signifies the effective bandwidth. It is calculated using the following formula:

$$TARC = \sqrt{\frac{\left(\left(\left|S_{11} + S_{12}e^{j\theta}\right|^2\right) + \left(\left|S_{21} + S_{22}e^{j\theta}\right|^2\right)\right)}{2}}. \quad (4)$$

Figure 19 shows the simulated and measured TARC of the proposed MIMO configuration. It is observed that the TARC is less than 10 dB for the operating frequency range from 22 GHz to 39 GHz, which validates the MIMO performance to be good.

7.4. Channel Capacity Loss (CCL). The CCL defines the maximum attainable limit with which the signal can be transmitted without substantial loss. The following set of equations is involved in calculating CCL.

$$CCL = -\log_2 \det(\alpha), \quad (5)$$

where $\alpha = \begin{vmatrix} \alpha_{11} & \alpha_{12} & \alpha_{13} & \alpha_{14} \\ \alpha_{21} & \alpha_{22} & \alpha_{23} & \alpha_{24} \\ \alpha_{31} & \alpha_{32} & \alpha_{33} & \alpha_{34} \\ \alpha_{41} & \alpha_{42} & \alpha_{43} & \alpha_{44} \end{vmatrix}$ and $\alpha_{ij} = 1 - (\sum_{j=1}^{M} |S_{ij}|^2)$.

The CCL calculated between antennas 1 and 2, 2 and 3, 3 and 4 is shown in Figure 20. The obtained CCL values are considerably less than the standard value of 0.4 bits/s/Hz as required for a MIMO antenna design.

8. Conclusion

A planar four-element MIMO antenna with decoupling lines is proposed for 5G mm Wave applications. The antenna structure is simple and compact occupying an area of 148.8 mm^3 ($13.75 \times 13.75 \times 0.787 mm^3$), and the frequency dependency on each parameter is emphasized in this article. The antenna resonates at 35 GHz with a -10 dB impedance bandwidth of 50.62% (23.9–40.1) GHz. The decoupling lines greatly reduce the isolation between the antennas from -20 $dB$to -30 dB. The calculated MIMO parameters such as ECC, DG, TARC, and CCL lie within the acceptable limits making the proposed structure suitable for wireless applications.

Data Availability

No data were used to support this study.

Conflicts of Interest

The authors declare no potential conflicts of interest.

References

[1] A. A. Althuwayb, M. J. Al-Hasan, A. Kumar, and D. Chaturvedi, "Design of halfmode substrate integrated cavity inspired dual-band antenna," *International Journal of RF and Microwave Computer-Aided Engineering*, vol. 31, no. 2, Article ID e22520, 2021.

[2] A. Kumar and S. Imaculate Rosaline, "Hybrid half-mode SIW cavity-backed diplex antenna for on-body transceiver applications," *Applied Physics A*, vol. 127, no. 11, p. 834 2021.

[3] A. Kumar and A. A. Althuwayb, "SIW resonator based duplex filtenna," *Antennas Wirel. Propag. Lett*, vol. 20, no. 12, pp. 2544–2548, 2021.

[4] D. Chaturvedi, A. Kumar, and S. Raghavan, "Wideband HMSIW-based slotted antenna for wireless fidelity application," *IET Microwaves, Antennas & Propagation*, vol. 13, no. 2, pp. 258–262, 2019.

[5] A. Kumar and S. Raghavan, "A design of miniaturized half-mode SIW cavity backed antenna," in *Proceedings of the 2016 IEEE Indian Antenna Week (IAW 2016)*, pp. 4–7, IEEE, Madurai, India, June 2016.

[6] J. Zhang, X. Ge, Q. Li, M. Guizani, and Y. Zhang, "5G millimeter-wave antenna array: design and challenges," *IEEE Wireless Communications*, vol. 24, no. 2, pp. 106–112, 2017.

[7] J. Huang, Y. Cao, X. Raimundo, A. Cheema, and S. Salous, "Rain statistics investigation and rain attenuation modeling for millimeter wave short-range fixed links," *IEEE Access*, vol. 24, no. 7, pp. 156110–156120, 2019.

[8] S. Joshi, S. Sancheti, and A. Goyal, "Rain attenuation measurements for short-range millimetre-wave radio link," *Electronics Letters*, vol. 42, no. 2, p. 72 2006.

[9] A. A. Al-Hadi, J. Ilvonen, R. Valkonen, and V. Viikari, "Eight-element antenna array for diversity and MIMO mobile terminal in LTE 3500 MHz band," *Microwave and Optical Technology Letters*, vol. 56, no. 6, pp. 1323–1327, 2014.

[10] N. Ojaroudi Parchin, H. Jahanbakhsh Basherlou, Y. I. A. Al-Yasir, A. Abdulkhaleq, M. Patwary, and R. A Abd-Alhameed, "A new CPW-Fed diversity antenna for MIMO 5G smartphones," *Electronics*, vol. 9, no. 2, p. 261 2020.

[11] A. Zhao and F. Ai, "5G mm-wave antenna array based on T-slot antenna for mobile terminals," in *Proceedings of the 2018 IEEE Asia-Pacific Conference on Antennas and Propagation (APCAP)*, pp. 476-477, IEEE, Auckland, New, August 2018.

[12] X. T. Yuan, Z. Chen, T. Gu, and T. Yuan, "A wideband PIFA-pair-based MIMO antenna for 5G smartphones," *IEEE Antennas and Wireless Propagation Letters*, vol. 20, no. 3, pp. 371–375, 2021.

[13] T. Jiang, T. Jiao, and Y. Li, "A low mutual coupling MIMO antenna using periodic multi-layered electromagnetic band gap structures," *Applied Computational Electromagnetics Society Journal*, vol. 33, no. 3, 2018.

[14] K. S. Parvathi and S. R. Gupta, "Novel dual-band EBG structure to reduce mutual coupling of air gap based MIMO antenna for 5G application," *AEU-International Journal of Electronics and Communications*, vol. 138, Article ID 153902, 2021.

[15] P. Rajat Girjashankar and T. Upadhyaya, "Substrate integrated waveguide fed dual band quad-elements rectangular dielectric resonator MIMO antenna for millimeter wave 5G wireless communication systems," *AEU-International Journal of Electronics and Communications*, vol. 137, Article ID 153821, 2021.

[16] Y. Zhang, J. Y. Deng, M. J. Li, D. Sun, and L. X. Guo, "A MIMO dielectric resonator antenna with improved isolation for 5G mm-wave applications," *IEEE Antennas and Wireless Propagation Letters*, vol. 18, no. 4, pp. 747–751, 2019.

[17] A. A. R. Saad and H. A. Mohamed, "Printed millimeter-wave MIMO-based slot antenna arrays for 5G networks," *AEU-International Journal of Electronics and Communications*, vol. 99, pp. 59–69, 2019.

[18] M. Venkateswara Rao, B. T. P. Madhav, J. Krishna, Y. Usha Devi, T. Anilkumar, and B. Prudhvi Nadh, "CSRR-loaded T-shaped MIMO antenna for 5G cellular networks and vehicular communications," *International Journal of RF and Microwave Computer-Aided Engineering*, vol. 29, no. 8, Article ID e21799, 2019.

[19] A. A. Althuwayb, "MTM-and SIW-inspired bowtie antenna loaded with AMC for 5G mm-wave applications," *International Journal of Antennas and Propagation*, vol. 2021, Article ID 6658819, 2021.

[20] S. F. Jilani, Q. H. Abbasi, M. A. Imran, and A. Alomainy, "Design and Analysis of Millimeter-Wave Antennas for the Fifth Generation Networks and Beyond," *Wiley 5G Ref: The Essential 5G Reference Online*, vol. 30, pp. 1–21, 2019.

[21] X. Zhang, Y. Li, W. Wang, and W. Shen, "Ultra-wideband 8-port MIMO antenna array for 5G metal-frame smartphones," *IEEE Access*, vol. 7, pp. 72273–72282, 2019.

[22] A. Kumar, S. Bhaskar, and A. K. Singh, "SIW cavity-backed U-shaped slot antenna for 5G applications," in *Proceedings of the 2019 IEEE Asia-Pacific Microwave Conference (APMC)*, pp. 1485–1487, IEEE, Singapore, December 2019.

[23] M. Ikram, E. A. Abbas, N. Nguyen-Trong, K. H. Sayidmarie, and A. Abbosh, "Integrated frequency-reconfigurable slot antenna and connected slot antenna array for 4G and 5G mobile handsets," *IEEE Transactions on Antennas and Propagation*, vol. 67, no. 12, pp. 7225–7233, 2019.

[24] M. Ikram, N. Nguyen-Trong, and A. Abbosh, "Hybrid antenna using open-ended slot for integrated 4G/5G mobile application," *IEEE Antennas and Wireless Propagation Letters*, vol. 19, no. 4, pp. 710–714, 2020.

[25] S. H. Kiani, A. Altaf, M. Abdullah et al., "Eight element side edged framed MIMO antenna array for future 5G smart phones," *Micromachines*, vol. 11, no. 11, p.956 2020.

[26] E. Yaacoub, M. Husseini, and H. Ghaziri, "An overview of research topics and challenges for 5G massive MIMO antennas," in *Proceedings of the 2016 IEEE Middle East Conference on Antennas and Propagation (MECAP)*, pp. 1–4, IEEE, Beirut, Lebanon, September 2016.

[27] L. Sun, H. Feng, Y. Li, and Z. Zhang, "Tightly arranged orthogonal mode antenna for 5G MIMO mobile terminal," *Microwave and Optical Technology Letters*, vol. 60, no. 7, pp. 1751–1756, 2018.

[28] L. Asadpor and M. Rezvani, "Multiband microstrip MIMO antenna with CSRR loaded for GSM and LTE applications," *Microwave and Optical Technology Letters*, vol. 60, no. 12, pp. 3076–3080, 2018.

[29] Z. Xu, Q. Zhang, and L. Guo, "A compact 5G decoupling MIMO antenna based on split-ring resonators," *International Journal of Antennas and Propagation*, vol. 2019, Article ID 3782528, 2019.

[30] Z. Ren, A. Zhao, and S. Wu, "MIMO antenna with compact decoupled antenna pairs for 5G mobile terminals," *IEEE Antennas and Wireless Propagation Letters*, vol. 18, no. 7, pp. 1367–1371, 2019.

[31] S. F. Jilani and A. Alomainy, "Millimetre-wave T-shaped MIMO antenna with defected ground structures for 5G cellular networks," *IET Microwaves Antennas & Propagation*, vol. 12, no. 5, pp. 672–677, 2018.

[32] A. Kumar and S. Raghavan, "Broadband dual-circularly polarised SIW cavity antenna using a stacked structure," *Electronics Letters*, vol. 53, no. 17, pp. 1171-1172, 2017.

[33] M. Wang, Y. Li, H. Zou, M. Peng, and G. Yang, "Compact MIMO antenna for 5G portable device using simple neutralization line structures," in *Proceedings of the 2018 IEEE International Symposium on Antennas and Propagation & USNC/URSI National Radio Science Meeting*, pp. 37-38, IEEE, Boston, MA, USA, July 2018.

[34] Y. T. Chen, Q. X. Chu, and H. L. Xu, "Two-antenna array with T-shaped neutralization line for 5G wideband application," in *Proceedings of the 2019 International Symposium on Antennas and Propagation (ISAP)*, pp. 1-2, IEEE, Xi'an, China, October 2019.

[35] A. Kumar, "Design of self-quadruplexing antenna using substrate-integrated waveguide technique," *Microwave and Optical Technology Letters*, vol. 61, no. 12, pp. 2687–2689, 2019.

[36] L. Sun, Y. Li, Z. Zhang, and H. Wang, "Self-decoupled MIMO antenna pair with shared radiator for 5G smartphones," *IEEE Transactions on Antennas and Propagation*, vol. 68, no. 5, pp. 3423–3432, 2020.

[37] R. Mathur and S. Dwari, "Compact 4-port UWB-MIMO slot antenna with dual polarization and low correlation for spatial diversity application," *Frequenz*, vol. 72, no. 11-12, pp. 503–509, 2018.

[38] A. Kumar and S. Raghavan, "Design of SIW cavity-backed self-triplexing antenna," *Electronics Letters*, vol. 54, no. 10, pp. 611-612, 2018.

[39] A. Kumar, A. A. Althuwayb, and M. J. Al-Hasan, "Wideband triple resonance patch antenna for 5G Wi-Fi spectrum," *Progress In Electromagnetics Research Letters*, vol. 93, pp. 89–97, 2020.

[40] A. Iqbal, M. Al-Hasan, I. B. Mabrouk, and M. Nedil, "A compact SIW based self-quadruplexing antenna for wearable transceivers," *IEEE Antennas and Wireless Propagation Letters*, vol. 20, no. 1, pp. 118–122, 2020.

[41] A. Iqbal, M. Al-Hasan, I. B. Mabrouk, A. Basir, M. Nedil, and H. Yoo, "Biotelemetry and wireless powering of biomedical implants using a rectifier integrated self-diplexing implantable antenna," *IEEE Transactions on Microwave Theory and Techniques*, vol. 69, no. 7, pp. 3438–3451, 2021.

[42] A. Kumar, D. Chaturvedi, and S. I. Rosaline, "Design of antenna-multiplexer for seamless on-body internet of medical things (IoMT) connectivity," *IEEE Transactions on Circuits and Systems II: Express Briefs*1 page, 2022.

[43] A. Iqbal, M. Al-Hasan, I. B. Mabrouk, and M. Nedil, "A compact implantable MIMO antenna for high data rate biotelemetry applications," *IEEE Transactions on Antennas and Propagation*, vol. 70, no. 1, pp. 631–640, 2021.

[44] N. Jaglan, S. D. Gupta, B. K. Kanaujia, and M. S. Sharawi, "10 element sub-6-GHz multi-band double-T based MIMO antenna system for 5G smartphones," *IEEE Access*, vol. 9, pp. 118662–118672, 2021.

[45] A. J. Alazemi and A. Iqbal, "A high data rate implantable MIMO antenna for deep implanted biomedical devices," *IEEE Transactions on Antennas and Propagation*, vol. 70, no. 2, pp. 998–1007, 2022.

[46] V. Thakur, N. Jaglan, and S. D. Gupta, "Side edge printed eight-element compact MIMO antenna array for 5G smartphone applications," *Journal of Electromagnetic Waves and Applications*, vol. 23, pp. 1–17, 2022.

[47] A. Iqbal, M. Al-Hasan, I. Mabrouk, and M. Nedil, "Scalp-implantable MIMO antenna for high-data-rate head implants," *IEEE Antennas and Wireless Propagation Letters*, vol. 20, no. 12, pp. 2529–2533, 2021.

[48] A. Iqbal, M. Al-Hasan, I. Mabrouk, and M. Nedil, "Scalp-Implantable MIMO antenna for high-data-rate head implants," *IEEE Antennas and Wireless Propagation Letters*, vol. 20, no. 12, pp. 2529–2533, 2021.

[49] N. Jaglan, S. D. Gupta, and M. S. Sharawi, "18 element massive MIMO/diversity 5G smartphones antenna design for sub-6 GHz LTE bands 42/43 applications," *IEEE Open Journal of Antennas and Propagation*, vol. 2, pp. 533–545, 2021.